remote sensing

Article

A Single-Site Vehicle Positioning Method in the Rectangular Tunnel Environment

Suying Jiang [1,2], Wei Wang [1,*] and Peng Peng [3]

1 School of Information Engineering, Chang'an University, Xi'an 710064, China
2 School of Electronic and Electrical Engineering, Baoji University of Arts and Sciences, Baoji 721013, China
3 School of Electrical and Control Engineering, Shaanxi University of Science and Technology, Xi'an 710021, China
* Correspondence: wei.wang@chd.edu.cn

Abstract: Due to the satellite signals are blocked, it is difficult to obtain the vehicle position in the tunnels. We propose a single-site vehicle localization scheme for the rectangular tunnel environment, where most satellite-based positioning methods can not provide the required localization accuracy. In the non-line-of-sight (NLOS) scenarios, we make use of the reflection paths as assistants for vehicle positioning. Specifically, first, the virtual stations are established based on the actual geometrical structure of the tunnel. Second, we use the direction-of-arrival (DOA) and time-of-arrival (TOA) information of reflection paths from two tunnel walls to achieve vehicle positioning. Especially, the Cramer-Rao lower bound (CRLB) of the joint TOA and DOA localization for NLOS propagations in a two-dimensional (2D) space is derived. In addition, based on the localization algorithms with and without filters, we assess the localization performance. In the line-of-sight (LOS) scenarios, we use the LOS path and two reflection paths from the tunnel walls to estimate the vehicle location. First, virtual base stations are established. Second, based on the obtained TOA information, different positioning algorithms are used to estimate the vehicle location. Simulation results illustrate that the proposed positioning approach can provide a small root mean square error. The localization algorithms using filters improve the localization accuracy, compared with the positioning algorithm without using filters, namely, the two-stage weighted least squares (TSWLS) algorithm. Moreover, the Unscented Particle Filter (UPF) algorithm achieves better positioning accuracy than other methods (i.e., Unscented Kalman Filter (UKF), Extended Kalman Filter (EKF), TSWLS algorithms).

Keywords: direction-of-arrival; single-site vehicle positioning; time-of-arrival; tunnel; virtual station

check for updates

Citation: Jiang, S.; Wang, W.; Peng, P. A Single-Site Vehicle Positioning Method in the Rectangular Tunnel Environment. *Remote Sens.* **2023**, *15*, 527. https://doi.org/10.3390/rs15020527

Academic Editors: Changhui Jiang, Yuwei Chen, Qian Meng, Panlong Wu, Bing Xu, Lianwu Guan, Wang Gao and Zeyu Li

Received: 29 November 2022
Revised: 9 January 2023
Accepted: 13 January 2023
Published: 16 January 2023

1. Introduction

Vehicular ad-hoc network (VANET) is a fundamental component of intelligent transportation system to improve road transport efficiency, reduce traffic accidents, and improve traffic safety [1,2]. VANET applications mainly include safety applications and comfort applications. The safety applications are conducive to improving vehicle and passengers' safety on the road. The comfort applications mainly include entertainment, commodity and online services, etc. [3–6]. VANETs implement these applications through vehicle-to-vehicle (V2V) and vehicle-to-infrastructure (V2I) communications. In VANETs, the vehicle has high mobility, and location-aware applications require updated and reliable position information. The inaccurate position information can seriously affect the effectiveness of the location-aware VANET applications. Therefore, vehicle position is one of the crucial information in VANET [6–10].

Due to vehicle mobility and the signal weakness resulting from environmental objects, it is challenging work to obtain the precise position of vehicles in VANETs. To overcome these difficulties, several locationing methods have been proposed to obtain vehicle location in VANET, such as Global Positioning System (GPS), dead reckoning, differential GPS, map matching, lateration techniques (i.e., distance-based lateration methods, angle-based lateration methods), filter-based techniques, cellular localization techniques, image/video processing techniques, roadside unit (RSU), etc. [6,7,11–13]. Many of the studies were appropriate for vehicle positioning in outdoor or indoor environments where GPS is available. However, GPS systems have faced undesirable issues. There are many scenarios without GPS signals, such as tunnels, canyons, parking garages, cities with large buildings, underground mines, etc. In these environments, GPS-based positioning methods can not achieve vehicle positioning. Vehicle positioning in these scenarios is very important and needs to be explored in depth [12]. In this paper, we aim to study vehicle localization technologies in tunnel scenarios.

Most research has focused on GPS-free vehicle localization methods for tunnel environments. The vehicle positioning technology in the tunnel environment mainly includes positioning techniques based on ultra-wideband (UWB), ZigBee, Light Detection and Ranging (LIDAR), Radio Frequency Identification (RFID), WiFi network positioning techniques, cooperative positioning, RSU-based positioning, visible light communication positioning, etc. In [14], the authors presented a localization scheme based on UWB for the vehicle in the tunnel. In [15], authors adopted UWB positioning technology and filtered the exceptional value during the measurement to improve positioning accuracy. In [16], a WiFi-based positioning method was adopted by the authors to achieve vehicle localization in the tunnel. In [17], the author proposed a facility–based vehicle positioning approach for highway tunnels exploiting 3D LIDAR. The tunnel facility points were obtained by exploiting LIDAR, and vehicle positions were estimated by the Extended Kalman Filter (EKF) based method. Moreover, several radio-ranging-based localization approaches are also widely adopted for vehicle localization in tunnels. In [18], the Received Signal Strength Indication (RSSI) localization approach based on the linear modified log function model was presented to improve the accuracy of RSSI positioning. In [19], authors proposed a time of arrival (TOA) and time difference of arrival (TDOA) based vehicle localization method in VANETs. These TOA-based methods are faced with the challenge of precise synchronization. In [20], authors proposed an automatic approach for the simultaneous refinement of the sensors' localizations and target position in the mine tunnel. In the paper, the TOA measurements based on UWB were used to acquire the target position. In [21], a cloud reasoning model-based positioning approach was proposed to realize the vehicle positioning inside the highway tunnel. In [22], authors proposed a novel grid-based on-road positioning scheme for the vehicle without GPS signal to compute target vehicle positions. Simulation results illustrate that the proposed positioning method has high positioning accuracy in tunnel and city environments. Some scholars use GPS signals outside the tunnel or pseudo-satellite technology to locate vehicles inside the tunnel. In [23], the magnetic field was used to calculate the target location inside a tunnel. In the proposed approach, before the vehicle enters the tunnels, the authors calibrated the sensors using location information from the global navigation satellite system (GNSS) and magnetic field database. In addition, the authors deployed the smartphone on the dashboard. Then the vehicle location was calculated by the authors exploiting the magnetic sensor of the phone.

To improve vehicular localization accuracy, the combination of localization information from different sources is considered, and the data fusion techniques (i.e., Particle Filter (PF), Kalman Filter (KF), Unscented Kalman Filter (UKF), EKF, etc.) are utilized to achieve high-accuracy localization. In [24], authors proposed a multi-sensor fusion approach to improve the vehicle localization performance in the tunnels. In the paper, the microelectromechanical system-based inertial sensor, electronic compass, RFID, and wheel speed sensor were integrated by the RFID-based positioning algorithm and the interacting multiple model-based global fusion method to obtain vehicle position.

Recently, many scholars have used V2V/V2I communication techniques to obtain vehicle positions in tunnels. In the V2I-based localization approach, each vehicle can estimate its location using the ranging measurements parameters (i.e., RSS, direction-of-arrival (DOA), TOA, and TDOA) transmitted from the surrounding RSUs or base stations (BSs). In [25], authors proposed a new cooperative localization scheme integrating V2I measurements with respect to RSUs. In [26], the existing V2I communication was used to obtain vehicle position in the tunnel environment. In the paper, the Doppler shift and TOA were considered by the authors, and EKF was adopted to incorporate the Doppler shift and TOA data. Results show that the EKF has a better positioning performance than Kalman Filter; it reduces the mean positioning error by 10 m. In [27], authors proposed a positioning system based on network connectivity of VANETs in road tunnels. The proposed positioning system includes two stages; specifically, first, the reference nodes are efficiently installed along the tunnel, with at least two reference nodes covering each vehicle; second, based on the data from reference nodes and adjacent vehicles, the network connectivity-based algorithm was used to estimate vehicle position. In [28], authors proposed a multipath-assisted positioning method to calculate the position of the mobile terminal. For the proposed positioning scheme, the authors used the Kalman filter to track the parameters of multipath components. Then the estimated multipath parameters and the heading information from an inertial measurement unit are used as input for the channel-simultaneous positioning and mapping algorithm to calculate the location of the mobile terminal. Based on the data obtained from outdoor measurements, the authors verified the effectiveness of the multipath-assisted positioning approach. In [28–32], authors studied various multipath-assisted positioning methods. To our knowledge, multipath-assisted positioning algorithms are not used to locate vehicles inside tunnels. These positioning strategies provide some new ideas for vehicle positioning in the tunnels, and they can be extended to vehicle localization in tunnels. However, the multipath-assisted positioning method has high complexity and is more difficult to implement. Table 1 gives a summary of various vehicle localization methods in the literature for the tunnels. As seen from the table, the commonly used localization algorithms in tunnels are EKF, UKF, etc.

Table 1. Vehicle localization methods in tunnel environments.

Reference	Method	Accuracy
[16]	WiFi, Open wireless positioning method	Less than 20 m
[24]	RFID, RSS, LMS, interactive multiple models, strong tracking EKF	Max: 2.98 m, RMS: 2.19 m
[33]	RFID, RSS, DR, least square support vector machine, federated UKF	2.91–4 m
[34]	Newton iteration location estimation, RSS, WSN	Less than 3 m
[35]	WSN, angle offset-assisted positioning	NA
[36]	Roadside LIDAR, inertial measurement unit	0.49 m
[37]	UWB, INS, EKF, residual weighting, factor graph model	0.5397 m
[14]	UWB	0.15–0.18 m
[20]	UWB, TOA	NA
[19]	TOA, time difference of arrival, onboard navigation unit, localization based on clustering in vehicular clouds	NA
[38,39]	Visible light communication, V2V, V2I	1 m
[25]	V2I, RSU, UWB, cooperative localization	0.1–2 m
[27]	V2V, V2I	9.16–14.5 m
[15]	UWB, exceptional Value Filtering, Greedy-based clustering algorithm	NA
[17]	3D LIDAR, EKF	Less than 0.2 m
[26]	Doppler shift, TOA, EKF	Max: 35.88 m, Mean: 20.3 m
[18]	RSSI, linear modified log function	1.95 m
[21]	Cloud reasoning model	Less than 1 m
[22]	A light-weight grid-based calculation mechanism	Less than 14 m
[23]	The magnetic sensor of a smartphone, magnetic sensor calibration method	9.33–30.38 m

To our knowledge, the V2I/V2V-based and multi-sensor data fusion positioning methods are widely used to calculate vehicle position. The V2V-based vehicle positioning method is founded on the transmission of location, speed, and direction information between the vehicles [40]. The successful transmission of information between vehicles depends on V2V communication. However, in real environments, due to adverse radio-frequency propagation and high vehicle dynamics, it is difficult to meet the required message update rate. Especially when the vehicle density is low, the V2V-based vehicle localization cannot meet the requirements. In tunnels, the vehicle density is usually low. In this case, only using the V2V positioning method cannot obtain accurate vehicle position. The data fusion and V2I-based positioning methods require the use of multiple sensors, RSUs, or base stations to achieve accurate vehicle positioning. Especially for the V2I-based positioning method, various factors have an influence on the vehicle positioning accuracy, for example, the number and positions of RSUs or base stations, the bandwidth dedicated for positioning, signal propagation conditions, etc. In V2I-based positioning methods, many RSUs or base stations are spatially separated at known positions to improve accuracy; this increases the cost of vehicle localization. In addition, it is not convenient to install many base stations or RSUs in the tunnel. Therefore, it is meaningful to use fewer base stations for precise vehicle positioning.

To simplify the complexity, reduce the cost, and improve the accuracy of vehicle positioning in the tunnel, we propose a single-site vehicle positioning scheme, which utilizes the TOA and DOA estimates for vehicle localization in a rectangular tunnel environment. In the proposed method, only one base station is used to achieve vehicle positioning in the tunnel. In addition, to improve the vehicle positioning accuracy, the Unscented Particle filter (UPF) is utilized to mitigate the channel propagation effects. In the proposed method, firstly, we build two virtual stations (VSs) based on the position of the base station and the structural characteristics of the tunnel. Secondly, we consider the reflection paths from the tunnel walls and convert the non-line-of-sight (NLOS) paths into line-of-sight (LOS) paths based on virtual station techniques. According to the geometric relationship between the VS and the base station, the path from the BS to the target vehicle is equivalent to the path from the VS to the target vehicle. Finally, for the NLOS cases, we can estimate the target vehicle position based on the DOA and TOA information of the reflection paths from the virtual stations. For the LOS cases, there are several methods to obtain vehicle locations. For example, we can obtain the target vehicle position based on the TOA information of the reflection paths from the virtual stations and the LOS path from the base station. We can also acquire the target vehicle position based on TOA and DOA information from the LOS and reflection paths. The contributions of this paper are summarized as follows:

- A novel single-site vehicle localization approach for the rectangular tunnel environment is proposed;
- The Cramer–Rao Lower Bound (CRLB) of joint TOA and DOA localization method is derived;
- The localization performance of the single-site vehicle localization method with and without filter under LOS and NLOS conditions are compared and analyzed.

The rest of the paper is organized as follows. Section 2, the establishment of virtual stations is described. The basic theory of single-site vehicle positioning and the joint TOA and DOA positioning method are described in Section 3. Moreover, we derive the CRLB of the proposed joint TOA and DOA vehicle positioning method. Section 4, we describe the two-stage weighted least squares (TSWLS) and UPF positioning algorithms. Section 5, we analyze the vehicular localization performance of the proposed single-site positioning scheme and compare the positioning performance of the single-site localization approach with and without a filter. In this section, the positioning performance of traditional TSWLS, EKF, UKF, and UPF algorithms for LOS and NLOS scenarios are compared. Finally, the concluding remarks are given in Section 6.

2. Establishment of Virtual Stations

It is known that the single-site positioning is an attractive positioning technique, which is simple to deploy, less costly, and easy to operate [41]. The positioning method does not require many base stations and is very suitable for vehicle positioning in a tunnel environment. In this paper, we aim to propose a two-dimensional (2D) single-site localization approach to calculate the target vehicle location in a rectangular tunnel. The BS is deployed at the entrance of the tunnel. In addition, the BS is deployed at a known location, and the position of the base station is denoted as $\mathbf{x_s} = [x_b, y_b]^T$. The BS transmits Orthogonal Frequency Division Multiplexing (OFDM) frames; the receivers receive OFDM frames from the fixed BS. Based on the obtained OFDM frames, the multipath TOA and the azimuth DOA can be obtained by channel parameter estimation algorithm [42,43]. The estimated parameters denote as $\hat{\theta}_i$, $\hat{\tau}_i$.

$$\hat{\theta}_i = \theta_i + n_{\theta_i}, \tag{1}$$

$$\hat{\tau}_i = \tau_i + n_{\tau_i}, \tag{2}$$

where θ_i denotes realistic arriving angle from the i-th VS to the vehicle, τ_i denotes realistic propagation delay from the i-th VS to the vehicle. n_{θ_i} denotes the measurement error of DOA; it is seen as zero-mean white Gaussian process with variance ${\sigma_{\theta_i}}^2$. n_{τ_i} denotes the measurement error of TOA; it is seen as zero-mean white Gaussian process with variance ${\sigma_{\tau_i}}^2$. n_{θ_i} and n_{τ_i} are assumed uncorrelated. Based on estimated delay $\hat{\tau}_i$, the estimated distance is calculated as $\hat{d}_i = c\hat{\tau}_i = d_i + n_{d_i}$. d_i represents the realistic distance between the virtual station i and the target vehicle. n_{d_i} denotes the distance measurement error of TOA, $n_{d_i} = cn_{\tau_i}$.

We suppose that the tunnel wall is a line, and the presentation of line l_1 can be written as $Ax + By + C_1 = 0$. For a tunnel, there are two tunnel walls; the other tunnel wall l_2 is denoted by $Ax + By + C_2 = 0$. The position of BS is $\mathbf{x_s} = [x_b, y_b]^T$. The position of the target vehicle node is $\mathbf{x_m} = [x, y]^T$. By calculating the symmetry point of the BS about the two tunnel walls, the locations of the two virtual stations can be obtained, as shown in Figure 1. In this paper, we focus on single-bounce reflecting NLOS path. The distance from BS to the target vehicle is equal to the distance from the virtual station to the target vehicle. By using the virtual station technique, the NLOS paths are converted into LOS paths for vehicle localization [44].

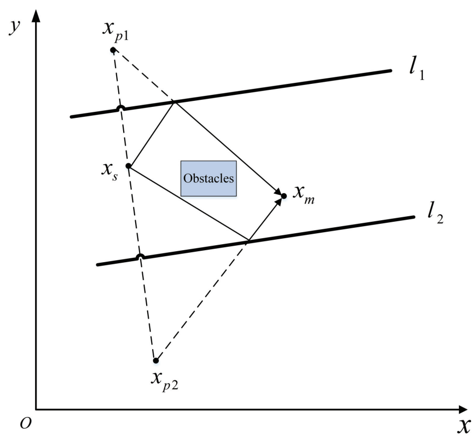

Figure 1. Single-bounce reflection paths and virtual stations.

The virtual station for the k-th reflection path from the tunnel wall is $\mathbf{x_{pk}} = [x_{vk}, y_{vk}]^T$. In Figure 1, the coordinates of virtual station $\mathbf{x_{p1}}$ and $\mathbf{x_{p2}}$ can be calculated as

$$\mathbf{x_{p1}} = \begin{bmatrix} x_{v1} \\ y_{v1} \end{bmatrix} = \begin{bmatrix} \frac{(B^2-A^2)x_b-2ABy_b-2AC_1}{A^2+B^2} \\ \frac{(A^2-B^2)y_b-2ABx_b-2BC_1}{A^2+B^2} \end{bmatrix}, \tag{3}$$

$$\mathbf{x_{p2}} = \begin{bmatrix} x_{v2} \\ y_{v2} \end{bmatrix} = \begin{bmatrix} \frac{(B^2-A^2)x_b - 2ABy_b - 2AC_2}{A^2+B^2} \\ \frac{(A^2-B^2)y_b - 2ABx_b - 2BC_2}{A^2+B^2} \end{bmatrix}. \tag{4}$$

The realistic arriving angle from the j-th virtual station to the target vehicle is θ_j, which is given by

$$\theta_j = \arctan\left(\frac{y - y_{vj}}{x - x_{vj}}\right), \tag{5}$$

where y_{vj} stands for the Y-axis coordinate of the virtual station j, x_{vj} is the X-axis coordinate of the virtual station j, x and y stand for the X-axis and Y-axis coordinates of the target vehicle, respectively.

3. Vehicle Localization Theory

3.1. Localization Methods in Different Scenarios

3.1.1. Vehicle Localization in LOS Scenarios

In the tunnel, there may be LOS or NLOS between the target vehicle and the base station. In the LOS case, the target vehicle position can be obtained based on the TOA parameters of the LOS path and the reflection paths from the tunnel walls. In addition, we can also acquire the vehicle location based on the DOA and TOA information of the reflection and LOS paths. In LOS scenarios, it is relatively easy to achieve the target vehicle localization. In this paper, we will not describe the implementation of the vehicle localization algorithm in the LOS scenarios in detail.

3.1.2. Vehicle Localization in NLOS Scenarios

In reality, due to the occlusion of other obstacles, NLOS often occurs between the target vehicle and the BS. Sometimes, there is no LOS path between the target vehicle and BS, as shown in Figure 2. The positioning of the target vehicle, in this case, is much more complicated than in LOS scenarios. In this case, we consider single-bounce reflection paths from the tunnel walls, convert the NLOS paths into LOS paths exploiting the virtual station technique, and then use different positioning algorithms to calculate the target vehicle position. The hybrid TOA and DOA values are used in the positioning algorithms.

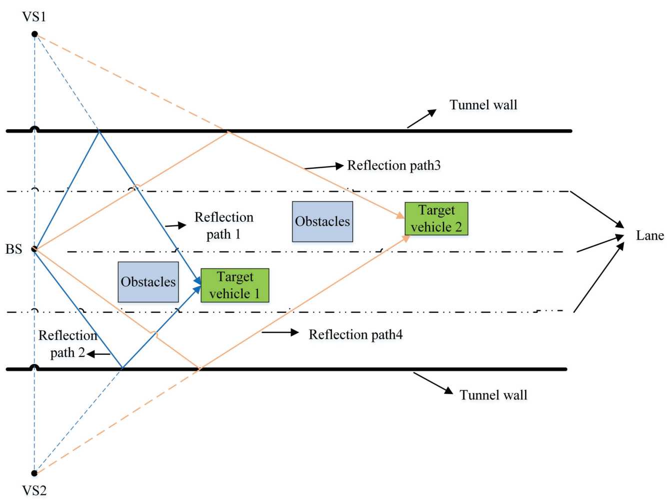

Figure 2. Vehicle localization based on reflecting paths from tunnel walls.

In addition to the method described above, the cooperative vehicle positioning approach can also be utilized to calculate the vehicle location. In Figure 3, the target vehicle 2 has a LOS path from BS. By applying the TOA parameters of the LOS path and two reflection paths from tunnel walls, we can obtain the localization of the target vehicle 2. In Figure 3, due to the obstruction of many obstacles, there is no LOS path between the target vehicle 1 and BS. We can achieve the target vehicle 1 localization according to the DOA and TOA information of the reflection paths from the tunnel walls and the surrounding vehicle. By using the TOA parameters of the two reflection paths from the tunnel walls and the reflection path from target vehicle 2, we can calculate the target vehicle 1 location based on the ranging method. By using the DOA and TOA parameters of any two reflection paths, we estimate the location of target vehicle 1.

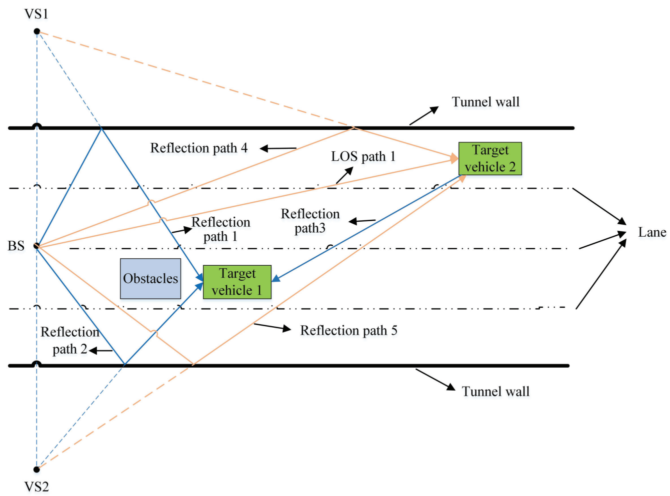

Figure 3. The cooperative vehicle positioning is based on reflecting paths from tunnel walls and surrounding vehicles.

3.2. Joint TOA and DOA Vehicle Localization

The possible location of the target vehicle is estimated based on the position of VS and the TOA and DOA parameters of reflection paths. It can be written as [45–47]:

$$\mathbf{x_m} = \begin{bmatrix} x \\ y \end{bmatrix} = \mathbf{x_{pi}} + \begin{bmatrix} c\hat{\tau}_i \cos\hat{\theta}_i \\ c\hat{\tau}_i \sin\hat{\theta}_i \end{bmatrix}, \tag{6}$$

where $\hat{\tau}_i$ denote the estimated TOA of i-th path, $\hat{\theta}_i$ denotes the estimated DOA of i-th path, $\mathbf{x_{pi}}$ is the coordinates of virtual station i, c represents the speed of light.

From Equation (5), we can obtain:

$$x \cdot \sin\theta_j - y \cdot \cos\theta_j = x_{vj} \cdot \sin\theta_j - y_{vj} \cdot \cos\theta_j. \tag{7}$$

The estimated arriving angle from the j-th virtual station to the target vehicle is $\hat{\theta}_j$, which is given by

$$\hat{\theta}_j = \arctan\left(\frac{y - y_{vj}}{x - x_{vj}}\right) + n_{\theta j}, \tag{8}$$

where $n_{\theta j}$ denotes the measurement error of DOA. From Equation (8), we can get

$$\tan(\hat{\theta}_j - n_{\theta j}) = \frac{y - y_{vj}}{x - x_{vj}}. \tag{9}$$

Combining Equations (9) and (6), we can get [44,45]

$$x \sin\hat{\theta}_j - y \cos\hat{\theta}_j = x_{vj} \sin\hat{\theta}_j - y_{vj} \cos\hat{\theta}_j + c\tau_j \sin(n_{\theta j}), \tag{10}$$

The estimated distance between the j-th VS and the target vehicle can be computed by

$$\hat{d}_j = d_j + n_{dj} = \sqrt{(x - x_{vj})^2 + (y - y_{vj})^2} + n_{dj}, \tag{11}$$

where d_j represents the realistic diatance between the virtual station j and target vehicle, n_{dj} denotes the distance measurement error of TOA, x_{vj} is the X-axis coordinate of the virtual station j, y_{vj} is the Y-axis coordinate of the virtual station j.

$$-2xx_{vj} - 2yy_{vj} + x^2 + y^2 = \left(\hat{d}_j - n_{dj}\right)^2 - {x_{vj}}^2 - {y_{vj}}^2. \tag{12}$$

Equations (10) and (12) are combined to obtain the following system of equations:

$$\mathbf{H} = \mathbf{GZ} + \mathbf{N}, \tag{13}$$

where

$$\mathbf{H} = \begin{bmatrix} \hat{d}_1^2 - {x_{v1}}^2 - {y_{v1}}^2 \\ \hat{d}_2^2 - {x_{v2}}^2 - {y_{v2}}^2 \\ x_{v1} \sin\hat{\theta}_1 - y_{v1} \cos\hat{\theta}_1 \\ x_{v2} \sin\hat{\theta}_2 - y_{v2} \cos\hat{\theta}_2 \end{bmatrix}, \tag{14}$$

$$\mathbf{G} = \begin{bmatrix} -2x_{v1} & -2y_{v1} & 1 \\ -2x_{v2} & -2y_{v2} & 1 \\ \sin\hat{\theta}_1 & -\cos\hat{\theta}_1 & 0 \\ \sin\hat{\theta}_2 & -\cos\hat{\theta}_2 & 0 \end{bmatrix}, \tag{15}$$

$$\mathbf{Z} = \begin{bmatrix} x \\ y \\ x^2 + y^2 \end{bmatrix}, \tag{16}$$

$$\mathbf{N} = \begin{bmatrix} {n_{d1}}^2 + 2d_1 n_{d1} \\ {n_{d2}}^2 + 2d_2 n_{d2} \\ -d_1 sin(n_{\theta 1}) \\ -d_2 sin(n_{\theta 2}) \end{bmatrix}. \tag{17}$$

3.3. Cramer-Rao Lower Bound

In this paper, the parameters of noise are perceived as independent and identically distributed Gaussian variables. Following this assumption, the probability of the above independent Gaussian variables is given by

$$\begin{aligned} \mathbf{f}\left(\mathbf{x_m} \middle| \hat{\boldsymbol{\theta}}, \hat{\boldsymbol{\tau}}\right) &= \prod_{i \in N} \frac{1}{\sqrt{2\pi{\sigma_{\theta_i}}^2}} \exp\left(-\frac{(\hat{\theta}_i - \theta_i)^2}{2{\sigma_{\theta_i}}^2}\right) \cdot \prod_{i \in N} \frac{1}{\sqrt{2\pi{\sigma_{d_i}}^2}} \exp\left(-\frac{\left(\hat{d}_i - d_i\right)^2}{2{\sigma_{d_i}}^2}\right) \\ &= \prod_{i \in N} \frac{1}{2\pi\sigma_{\theta_i}\sigma_{d_i}} \exp\left(-\left(\frac{(\hat{\theta}_i - \theta_i)^2}{2{\sigma_{\theta_i}}^2} + \frac{\left(\hat{d}_i - d_i\right)^2}{2{\sigma_{d_i}}^2}\right)\right), \end{aligned} \tag{18}$$

where N represents the number of single-bounce reflection paths. In this paper, we consider two reflection paths from the tunnel walls, therefore $N = 2$.

The log-likelihood function is given by

$$L = \sum_{i=1}^{N} \ln\left(\frac{1}{2\pi\sigma_{\theta_i}\sigma_{d_i}}\right) - \sum_{i=1}^{N} \frac{1}{2}\left(\frac{(\hat{\theta}_i - \theta_i)^2}{{\sigma_{\theta_i}}^2} + \frac{\left(\hat{d}_i - d_i\right)^2}{{\sigma_{d_i}}^2}\right). \tag{19}$$

The CRLB determines the theoretical lower bound for the performance of an unbiased estimator. Generally, it is specified as the inverse of the Fischer Information Matrix (FIM), which can be obtained from the above log-likelihood function L as [48]:

$$\mathbf{F} = \begin{bmatrix} F_{xx} & F_{xy} \\ F_{yx} & F_{yy} \end{bmatrix}, \tag{20}$$

with

$$F_{xx} = -\mathrm{E}\left\{\frac{\partial^2 L}{\partial^2 x}\right\}, \tag{21}$$

$$F_{xy} = -\mathrm{E}\left\{\frac{\partial\left(\frac{\partial L}{\partial x}\right)}{\partial y}\right\}, \tag{22}$$

$$F_{yx} = -\mathrm{E}\left\{\frac{\partial\left(\frac{\partial L}{\partial y}\right)}{\partial x}\right\}, \tag{23}$$

$$F_{yy} = -\mathrm{E}\left\{\frac{\partial^2 L}{\partial^2 y}\right\}. \tag{24}$$

After calculation, we obtain

$$F_{xx} = \sum_{i=1}^{N}\left(\frac{(y-y_{vi})^2}{{\sigma_{\theta i}}^2{d_i}^4}\right) + \sum_{i=1}^{N}\left(\frac{(x-x_{vi})^2}{{\sigma_{di}}^2{d_i}^2}\right), \tag{25}$$

$$F_{yy} = \sum_{i=1}^{N}\left(\frac{(x-x_{vi})^2}{{\sigma_{\theta i}}^2{d_i}^4}\right) + \sum_{i=1}^{N}\left(\frac{(y-y_{vi})^2}{{\sigma_{di}}^2{d_i}^2}\right), \tag{26}$$

$$F_{xy} = F_{yx} = \sum_{i=1}^{N}\left(\frac{(x-x_{vi})(y-y_{vi})}{{\sigma_{\theta i}}^2{d_i}^4}\right) + \sum_{i=1}^{N}\left(\frac{(x-x_{vi})(y-y_{vi})}{{\sigma_{di}}^2{d_i}^2}\right). \tag{27}$$

Appendix A gives the details on the derivation of CRLB.

The root mean squared error (RMSE) of the vehicle localization is described by

$${\sigma_M}^2 \geq tr\left(\mathbf{F}^{-1}\right). \tag{28}$$

4. The Positioning Algorithm

Various localization algorithms can be used to locate vehicles in tunnels, such as the algorithms without filter (TSWLS, WLS), the filtering algorithm (e.g., KF, EKF, PF, UKF, etc.), etc. To enhance vehicle localization performance, we exploit UPF to estimate vehicle position. Moreover, we will analyze the localization performance of various algorithms with and without filters. When the filter is not used, we directly use the TSWLS algorithm to locate the target vehicle. When the filter is used, we use the UPF algorithm to locate the target vehicle. In the following, these two algorithms are described in detail.

4.1. TSWLS

From (13), we find that the noise term is nonlinear Gaussian noise. Due to $n_{\theta j}$ and n_{di} are usually very small, many scholars approximate the noise term in the (13) as Gaussian noise. Then the TSWLS algorithm is usually used to obtain the solution of (13).

When $n_{\theta j}$ is small, we consider $\sin(n_{\theta j}) \approx n_{\theta j}$. In general, ${n_{di}}^2$ can be ignored [49], therefore, $\mathbf{N}$ can be rewritten as

$$\mathbf{N} = \begin{bmatrix} 2d_1 n_{d1} \\ 2d_2 n_{d2} \\ -d_1 n_{\theta 1} \\ -d_2 n_{\theta 2} \end{bmatrix}. \tag{29}$$

In the first step of TSWLS, the unknown vector $\mathbf{Z}$ can be obtained from the weighted least square (WLS) solution of Equation (13),

$$\hat{\mathbf{Z}} = \left(\mathbf{G}^T \mathbf{W}^{-1} \mathbf{G}\right)^{-1} \mathbf{G}^T \mathbf{W}^{-1} \mathbf{H}, \tag{30}$$

where $\mathbf{W} = \mathrm{E}\left[\mathbf{N}\mathbf{N}^{\mathbf{T}}\right] = \mathbf{BQB}$, with

$$\mathbf{B} = \begin{bmatrix} 2d_1 & 0 & 0 & 0 \\ 0 & 2d_2 & 0 & 0 \\ 0 & 0 & d_1 & 0 \\ 0 & 0 & 0 & d_2 \end{bmatrix}, \tag{31}$$

$$\mathbf{Q} = \begin{bmatrix} {\delta_{d_1}}^2 & 0 & 0 & 0 \\ 0 & {\delta_{d_2}}^2 & 0 & 0 \\ 0 & 0 & {\delta_{\theta_1}}^2 & 0 \\ 0 & 0 & 0 & {\delta_{\theta_2}}^2 \end{bmatrix}. \tag{32}$$

To obtain $\mathbf{B}$, we usually use the estimated $\hat{d}_j$ instead of the realistic d_j. Therefore, the parameters in $\mathbf{B}$ can be obtained from the estimated TOA and DOA information. The parameters in $\mathbf{Q}$ depend on the variances of the collected data, which are difficult to obtain [44].

In the second step, according to the relation between (x, y) and $x^2 + y^2$, we can construct the following system of equations:

$$\mathbf{G_1 Z_1} = \mathbf{H_1} + \mathbf{N_1}, \tag{33}$$

where

$$\mathbf{G_1} = \begin{bmatrix} 1 & 0 \\ 0 & 1 \\ 1 & 1 \end{bmatrix}, \tag{34}$$

$$\mathbf{Z_1} = \begin{bmatrix} x^2 \\ y^2 \end{bmatrix}, \tag{35}$$

$$\mathbf{H_1} = \begin{bmatrix} \hat{x}^2 \\ \hat{y}^2 \\ \hat{x}^2 + \hat{y}^2 \end{bmatrix}, \tag{36}$$

$$\mathbf{N_1} = \begin{bmatrix} x^2 - \hat{x}^2 \\ y^2 - \hat{y}^2 \\ x^2 + y^2 - (\hat{x}^2 + \hat{y}^2) \end{bmatrix}. \tag{37}$$

The unknown vector $\mathbf{Z_1}$ can be calculated by

$$\hat{\mathbf{Z}}_\mathbf{1} = \left({\mathbf{G_1}}^T {\mathbf{W_1}}^{-1} \mathbf{G_1}\right)^{-1} {\mathbf{G_1}}^T {\mathbf{W_1}}^{-1} \mathbf{H_1}, \tag{38}$$

where $\mathbf{W_1} = \mathrm{E}\left[\mathbf{N_1}{\mathbf{N_1}}^{\mathbf{T}}\right] = 4\mathbf{B_1}\left(\mathbf{G^T W^{-1} G}\right)^{-1}\mathbf{B_1}$, with $\mathbf{B_1} = diag\{\hat{x}, \hat{y}, 0.5\}$.

Finally, the target vehicle position is calculated by

$$\hat{\mathbf{x}}_{\mathbf{m}} = diag\{s\hat{g}n([\hat{\mathbf{Z}}(1), \hat{\mathbf{Z}}(2)])\}\sqrt{\hat{\mathbf{Z}}_{\mathbf{1}}}, \tag{39}$$

where **sgn** denotes the sign function.

4.2. The Positioning Algorithm Based on UPF

The PF algorithm is not limited by linearization error or Gaussian noise assumption; it is applicable to nonlinear non-Gaussian random systems. However, in the particle filter algorithm, the current measurement value is not taken into account when selecting the importance density function; therefore, there is a large deviation between the importance function based on prior distribution and the real posterior probability density function (PDF). Therefore, the key to the design of a particle filter is to select a reasonable importance density function. Incorporating current observations is the easiest way to improve the importance density function [50]. The UPF algorithm considers the current observed values and exploits the UKF algorithm to generate the proposal distributions, which can make the proposal distribution function close to the real distribution of the target PDF, make the importance density function more reasonable, and improve the filtering accuracy of the PF [50–52]. The UPF algorithm is used to solve parameter estimation and state filtering problems for nonlinear and non-Gaussian systems. Therefore, we propose the joint TOA-DOA fusion localization algorithm based on UPF to locate the target vehicle.

4.2.1. System Model

In the paper, it is assumed that the target vehicle moves along a straight line with uniform velocity in the tunnel. Therefore, the state equation of the vehicle is expressed as

$$\mathbf{X}_{\mathbf{k}} = \mathbf{\Phi}\mathbf{X}_{\mathbf{k-1}} + \boldsymbol{U}_{\boldsymbol{k-1}}, \tag{40}$$

where $\boldsymbol{U}_{\boldsymbol{k-1}}$ represents the process noise vector, $\boldsymbol{U}_k \sim N(0, \boldsymbol{Q}_k)$, $\boldsymbol{Q}_k$ denotes the covariance matrix of the process noise vector. We consider the vehicle positioning in two dimensions. $\boldsymbol{X}_{\boldsymbol{k}}$ stands for the state value of the target vehicle at time k; it is n-dimensional state vector. In this paper, $\boldsymbol{X}_{\boldsymbol{k}} = [x_k, y_k, \dot{x}_k, \dot{y}_k]^T$, therefore $n = 4$. $\mathbf{\Phi}$ denotes the state transition matrix; it can be calculated by

$$\mathbf{\Phi} = \begin{bmatrix} 1 & 0 & T_1 & 0 \\ 0 & 1 & 0 & T_1 \\ 0 & 0 & 1 & 0 \\ 0 & 0 & 0 & 1 \end{bmatrix}, \tag{41}$$

where T_1 is the observation period. The Equation (40) is written as $\mathbf{X}_{\mathbf{k}} = f_1(\mathbf{X}_{\mathbf{k-1}}) + \boldsymbol{U}_{\boldsymbol{k-1}}$.

We assume that the distance between the i-th VS and the target vehicle can be defined as d_{ik}, the azimuth angle of the target vehicle at time k with respect to the i-th VS is β_{ik}. Then, β_{ik} and d_{ik} can be obtained as

$$\beta_{ik} = \arctan\frac{y_k - y_{vi}}{x_k - x_{vi}}, \tag{42}$$

$$d_{ik} = \sqrt{(x_k - x_{vi})^2 + (y_k - y_{vi})^2}, \tag{43}$$

where (x_k, y_k) denotes the coordinate of the target vehicle at time k, (x_{vi}, y_{vi}) is the coordinate of the i-th VS.

The system observation model can be obtained as

$$\mathbf{Z}_{\mathrm{k}} = \mathrm{f}_2(\mathbf{X}_{\mathrm{k}}) + \mathbf{V}_{k-1}, \tag{44}$$

where $\mathbf{V}_{k-1}$ denotes the observation noise, $\boldsymbol{V}_k \sim N(0, \boldsymbol{R}_k)$, $\boldsymbol{R}_k$ denotes the covariance matrix of the observation noise. $\mathrm{f}_2(\mathbf{X}_\mathrm{k})$ can be expressed as

$$\mathrm{f}_2(\mathbf{X}_\mathrm{k}) = \begin{bmatrix} \sqrt{(x_k - x_{v1})^2 + (y_k - y_{v1})^2} \\ \sqrt{(x_k - x_{v2})^2 + (y_k - y_{v2})^2} \\ \arctan\left(\frac{y_k - y_{v1}}{x_k - x_{v1}}\right) \\ \arctan\left(\frac{y_k - y_{v2}}{x_k - x_{v2}}\right) \end{bmatrix}, \tag{45}$$

where (x_{v1}, y_{v1}) and (x_{v2}, y_{v2}) are the coordinates of the first VS and the second VS, respectively. (x_k, y_k) stands for the coordinate of the target vehicle.

4.2.2. UPF

The UPF algorithm consists of the following main steps.

(1) Initialization ($k = 0$): for $i = 1, 2, ..., N_1$, generate particle $X_0^i \sim p(X_0)$. Then set $k = 1$.

(2) Calculate sigma points. Generate $2n_x + 1$ sigma points and their weights according to the following:

$$X_{k-1}^i = \left[\bar{X}_{k-1}^i, \bar{X}_{k-1}^i \pm \sqrt{(n_x + \lambda) P_{k-1}^i}\right], \tag{46}$$

$$\omega_0^{(m)} = \frac{\lambda}{n_x + \lambda}, \tag{47}$$

$$\omega_0^{(c)} = \frac{\lambda}{n_x + \lambda} + \left(1 - \alpha^2 + \beta\right), \tag{48}$$

$$\omega_i^{(m)} = w_i^{(c)} = \frac{1}{2(n_x + \lambda)} \quad i = 1 \ldots 2n_x, \tag{49}$$

$$\lambda = \alpha^2 (n_x + \kappa) - n_x, \tag{50}$$

where P_{k-1}^i is the covariance of X_{k-1}. α denotes a positive scaling parameter; it determines the spread of the sigma points around $\bar{X}$, it is a small value. β can be utilized to incorporate prior knowledge of the distribution of X. κ represents a secondary scaling parameter. λ represents a scaling parameter.

(3) The UKF method is applied to compute the mean and covariance of particles. Time update equations are given by

$$X_{k|k-1}^i = f_1\left(X_{k-1}^i\right) + U_{k-1}, \quad \bar{X}_{k|k-1}^i = \sum_{i=0}^{2n_x} \omega_i^{(m)} X_{k|k-1}^i, \tag{51}$$

$$P_{k|k-1} = \sum_{i=0}^{2n_x} \omega_i^{(c)} \left[X_{k|k-1}^i - \bar{X}_{k|k-1}^i\right] \left[X_{k|k-1}^i - \bar{X}_{k|k-1}^i\right]^T + Q_k. \tag{52}$$

$$Z_{k|k-1}^i = f_2\left(X_{k|k-1}^i\right) + V_{k-1}, \quad \bar{Z}_{k|k-1}^i = \sum_{i=0}^{2n_x} \omega_i^{(m)} Z_{k|k-1}^i, \tag{53}$$

The measurement update equations can be written as

$$\bar{X}_k^i = \bar{X}_{k|k-1}^i + K_k\left(Z_k - \bar{Z}_{k|k-1}^i\right), \tag{54}$$

$$P_k^i = P_{k|k-1}^i - K_k P_{z_k z_k} (K_k)^T, \tag{55}$$

where

$$P_{z_k z_k} = \sum_{i=0}^{2n_x} \omega_i^{(c)} \left[Z_{k|k-1}^i - \bar{Z}_{k|k-1}^i \right] \left[Z_{k|k-1}^i - \bar{Z}_{k|k-1}^i \right]^T + R_k, \tag{56}$$

$$P_{x_k z_k} = \sum_{i=0}^{2n_x} \omega_i^{(c)} \left[X_{k|k-1}^i - \bar{X}_{k|k-1}^i \right] \left[Z_{k|k-1}^i - \bar{Z}_{k|k-1}^i \right]^T, \tag{57}$$

$$K_k = P_{x_k z_k} (P_{z_k z_k})^{-1}, \tag{58}$$

where K denotes the Kalman gain matrix at step k.

(4) Importance sampling: sample particles according to the importance density function.

$$X_k^i \sim q\left(X_k^i \mid X_{0:(k-1)}^i, Z_{1:k} \right) = N(\bar{X}_k^i, P_k^i) \tag{59}$$

(5) Update particles weights: for $i = 1, 2, ..., N_1$, calculate and normalize the importance weights.

$$\omega_k^i = \omega_{k-1}^i \frac{p(Z_k \mid X_k^i) p\left(X_k^i \mid X_{k-1}^i \right)}{q\left(X_k^i \mid X_{0:(k-1)}^i, Z_{1:k} \right)}, \tag{60}$$

$$\bar{\omega}_k^i = \omega_k^i / \sum_{i=1}^{N_1} \omega_k^i, \tag{61}$$

(6) Resampling: the particles with low weights are eliminated. The particle with large weights is duplicated. Obtain a new set of particles $\{X_k^i, \omega_k^i\}$ by resampling. Then set $\bar{\omega}_k^i = 1/N_1$.

(7) Output:

$$\hat{X}_k^i = \sum_{i=1}^{N_1} \bar{\omega}_k^i X_k^i \tag{62}$$

$$P_k^i = \sum_{i=1}^{N_1} \bar{\omega}_k^{(i)} \left(X_k^i - \hat{X}_k^i \right) \left(X_k^i - \hat{X}_k^i \right)^T \tag{63}$$

(8) Let $k = k + 1$, go to 2.

5. Simulation Results

In this section, we aim to validate and analyze the localization performance of the proposed single-site positioning scheme. First, we directly estimate the vehicle location using the TSWLS algorithm. Then, we estimate the vehicle location using different filters, such as EKF, UKF, and UPF. Finally, we analyze the positioning performance of the proposed single-site localization approach with and without filters in different scenarios.

In the simulations, the experiment is repeated 100 times independently. The localization performance is evaluated by computing the RMSE, which is calculated by [53]:

$$\text{RMSE} = \sqrt{\frac{1}{l} \sum_{i=1}^{l} \|\hat{\mathbf{x}}_m - \mathbf{x}_m\|^2 \ }|, \tag{64}$$

where $\mathbf{x}_m$ is the realistic position of the vehicle, $\hat{\mathbf{x}}_m$ denotes the estimated target vehicle position, l stands for the number of times the simulation experiment was executed.

In the simulations, to generate data, the following scenarios are taken into account. We take the length of the tunnel as the X-axis and the width of the tunnel as the Y-axis, and a two-dimensional coordinate system is established. We assume the tunnel walls can be seen as two lines, namely, $3x - 3y + 40 = 0$ and $3x - 3y - 23.6396 = 0$. The position of BS is $(0, 0)$. In this paper, we consider two cases. In the first case, the vehicle moves uniformly along a straight line in the tunnel. The starting point coordinate of the vehicle is

$(10, 14.8481)$, and the speed is 14.1421 m/s. In the second case, the vehicle makes uniform acceleration and uniform deceleration motion in the tunnel, and the trajectory of the vehicle is curved. The starting point coordinate of the vehicle is $(10, 6.3628)$.

5.1. NLOS Scenarios

In NLOS scenarios, we estimate the vehicle position using the joint TOA and DOA localization methods. In the proposed single-site positioning method, only one base station is needed to obtain the vehicle location.

5.1.1. Straight Line Trajectory

In the following, we analyze the localization performance of different algorithms assuming that the vehicle moves uniformly along a straight line in the tunnel.

Figure 4 shows the RMSEs of different algorithms for $\sigma_{\theta_i} = 0.5^\circ$, $\sigma_{d_i} = 0.1$ m. Simulation results illustrate that the proposed single base station localization scheme can effectively realize vehicle localization for the tunnel environment in NLOS scenarios. In addition, it is shown that the UPF approach has the best localization accuracy. The positioning method using the filter can effectively improve positioning accuracy.

Figure 5 provides the cumulative distribution function (CDF) of RMSE using different algorithms for $\sigma_{\theta_i} = 0.5^\circ$, $\sigma_{d_i} = 0.1$ m. Simulation results show that when the RMSE is constant, the CDF of RMSE for the UPF algorithm is larger than in other methods. Therefore, the UPF localization performance is better than EKF, UKF, and TSWLS algorithms.

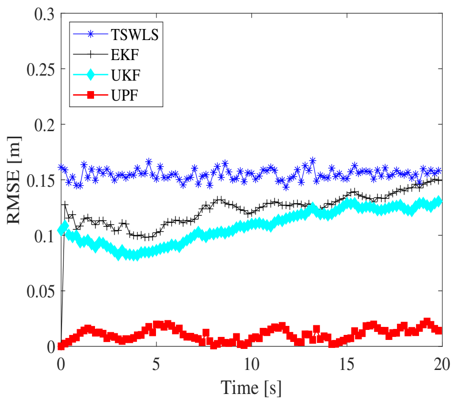

Figure 4. The RMSE of different algorithms in NLOS scenario ($\sigma_{\theta_i} = 0.5^\circ$, $\sigma_{d_i} = 0.1$ m).

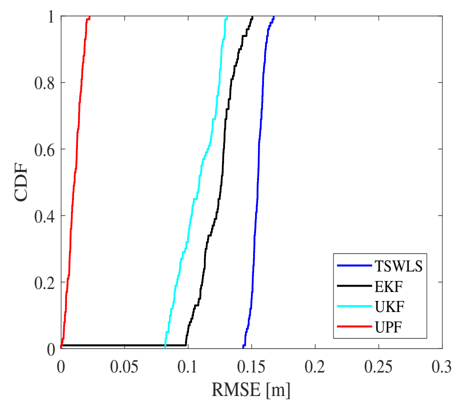

Figure 5. The CDF of RMSE for different methods in NLOS scenario ($\sigma_{\theta_i} = 0.5^\circ$, $\sigma_{d_i} = 0.1$ m).

Figures 6 and 7 show the RMSE and the CDF of RMSE for $\sigma_{\theta_i} = 1^\circ$, $\sigma_{d_i} = 1$ m. Figures 8 and 9 show the RMSE and the CDF of RMSE for $\sigma_{\theta_i} = 2^\circ$, $\sigma_{d_i} = 2$ m. When the measurement errors are relatively large, the proposed single-site positioning method can be utilized to calculate vehicle position effectively. These results validate that the positioning performance of the UPF algorithm is better than other algorithms.

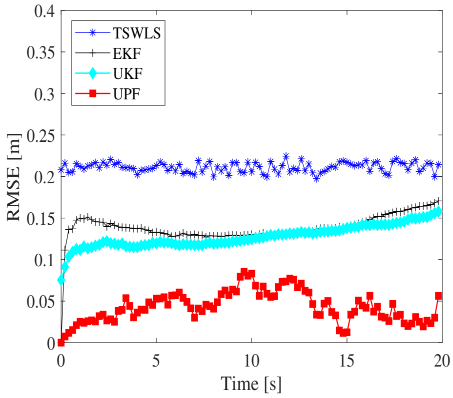

Figure 6. The RMSE of different algorithms in NLOS scenario ($\sigma_{\theta_i} = 1^\circ$, $\sigma_{d_i} = 1$ m).

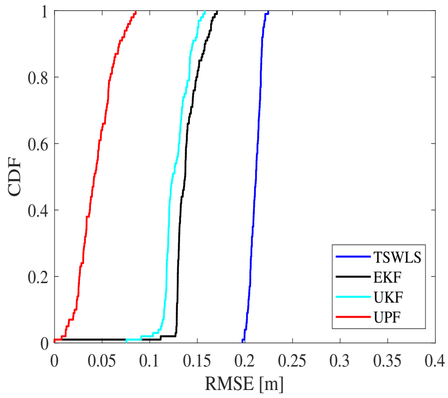

Figure 7. The CDF of RMSE for different algorithms in NLOS scenario ($\sigma_{\theta_i} = 1^\circ$, $\sigma_{d_i} = 1$ m).

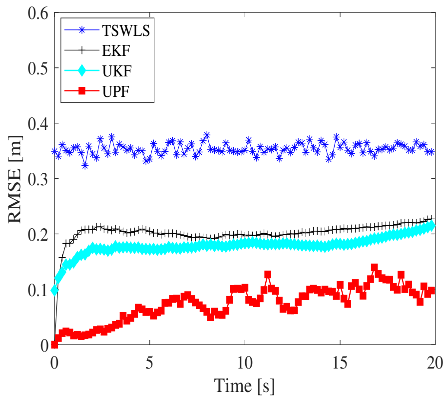

Figure 8. The RMSE of different algorithms in NLOS scenario ($\sigma_{\theta_i} = 2^\circ$, $\sigma_{d_i} = 2$ m).

Table 2 presents the statistical parameters of positioning error in NLOS scenarios. When setting different standard deviations of angle and distance, we calculate the mean and variance of positioning error. The UPF algorithm has the smallest mean value of positioning error. The TSWLS algorithm has the smallest variance of positioning error. The UPF algorithm has better positioning performance than other algorithms. Moreover, we find that the vehicle positioning performance is related to the measurement errors of TOA and DOA. It is shown that the greater the measurement error, the greater the positioning error. This finding is consistent with the conclusions in [44,54].

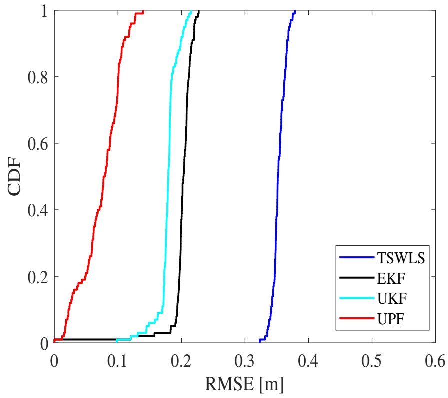

Figure 9. The CDF of RMSE for different algorithms in NLOS scenario ($\sigma_{\theta_i} = 2°$, $\sigma_{d_i} = 2$ m).

Table 2. The statistical parameters of positioning error in NLOS scenarios.

Algorithm	$\sigma_{\theta_i} = 0.5°$, $\sigma_{d_i} = 0.1$ m		$\sigma_{\theta_i} = 1°$, $\sigma_{d_i} = 1$ m		$\sigma_{\theta_i} = 2°$, $\sigma_{d_i} = 2$ m	
	Mean [m]	**Variance**	**Mean [m]**	**Variance**	**Mean [m]**	**Variance**
TSWLS	0.1455	0.0059	0.1991	0.0067	0.3330	0.0118
EKF	0.1004	0.0138	0.1210	0.0158	0.1765	0.0212
UKF	0.0896	0.0108	0.1129	0.0126	0.1596	0.0149
UPF	0.0110	0.0057	0.0432	0.0185	0.0742	0.0316

5.1.2. Curved Trajectory

In the following, we analyze the positioning performance of different algorithms assuming that the trajectory of the target vehicle in the tunnel is a curve. Figure 10 shows the estimated positions of the vehicle and the real positions of the vehicle. The result illustrates that the joint TOA and DOA localization approach using UPF can accurately estimate the location of the vehicle.

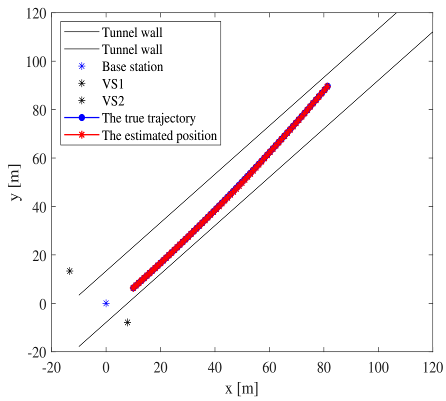

Figure 10. The positioning performance of the UPF in NLOS scenario ($\sigma_{\theta_i} = 2°$, $\sigma_{d_i} = 2$ m).

Figure 11 and 12 show the RMSE and the CDF of RMSE for $\sigma_{\theta_i} = 2°$, $\sigma_{d_i} = 2$ m. When the trajectory of the target vehicle is curved, the proposed single-site positioning method can be utilized to effectively calculate vehicle position even if the measurement errors are relatively large. In addition, the results illustrate that the localization performance of the UPF algorithm is better than the other algorithms.

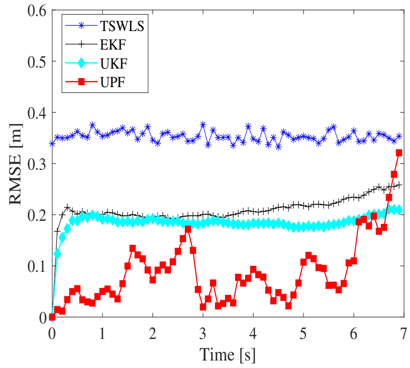

Figure 11. The RMSE of different algorithms in NLOS scenario ($\sigma_{\theta_i} = 2^\circ$, $\sigma_{d_i} = 2$ m).

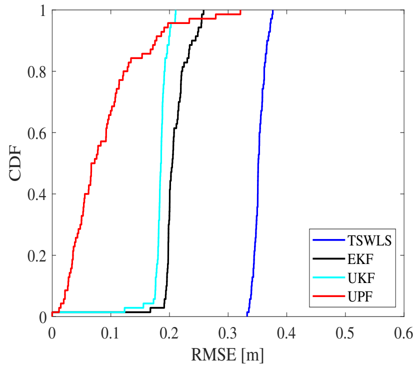

Figure 12. The CDF of RMSE for different algorithms in NLOS scenario ($\sigma_{\theta_i} = 2^\circ$, $\sigma_{d_i} = 2$ m).

5.2. LOS Scenarios

In LOS scenarios, we estimate the vehicle position using the joint TOA and DOA positioning algorithm. Using the delay and angle information of different paths (i.e., the LOS path from the base station and two reflection paths from the tunnel walls), we calculate vehicle location using different algorithms.

5.2.1. Straight Line Trajectory

In the following, we analyze the localization performance of different algorithms assuming that the vehicle moves uniformly in a straight line in the tunnel.

Figures 13–15 show the RMSE of different algorithms for different measurement errors in LOS scenarios. Results indicate that the proposed single base station localization approach can effectively achieve vehicle position in the LOS scenarios. The UPF algorithm has better localization performance than other algorithms in most cases.

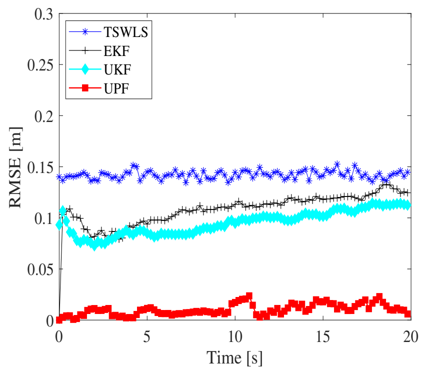

Figure 13. The RMSE of different algorithms in LOS scenario ($\sigma_{\theta_i} = 0.5^\circ$, $\sigma_{d_i} = 0.1$ m).

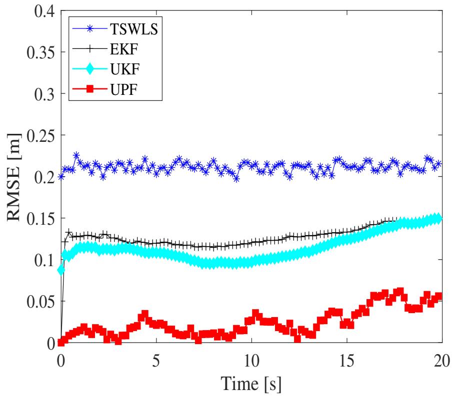

Figure 14. The RMSE of different algorithms in LOS scenario ($\sigma_{\theta_i} = 1^\circ$, $\sigma_{d_i} = 1$ m).

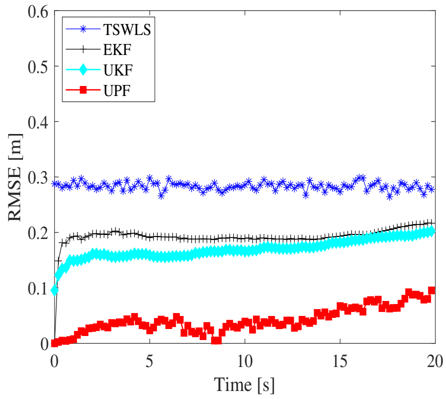

Figure 15. The RMSE of different algorithms in LOS scenario ($\sigma_{\theta_i} = 2^\circ$, $\sigma_{d_i} = 2$ m).

Figures 16–18 provide the CDF of RMSE using different algorithms for different measurement errors in LOS scenarios. The RMSE of the UPF algorithm is smaller than other methods in most cases. The UPF positioning performance is better than the EKF, UKF, and TSWLS algorithms.

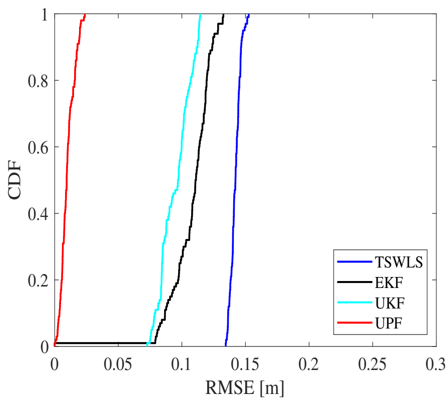

Figure 16. The CDF of RMSE for different algorithms in LOS scenario ($\sigma_{\theta_i} = 0.5^\circ$, $\sigma_{d_i} = 0.1$ m).

Table 3 illustrates the statistical parameters of positioning error for different standard deviations of angle and distance in LOS scenarios. From the table, we find that the UPF algorithm has the smallest mean of positioning error. Therefore, the UPF algorithm has the best vehicle positioning performance. In addition, the positioning methods using filters have a smaller mean of positioning error than the positioning method without using filters (i.e., the TSWLS algorithm). The positioning performance of the positioning methods using filters is better than the positioning method without using filters, namely, the TSWLS algorithm. We theoretically show that effective vehicle localization can be achieved in tunnels using the single-site localization method.

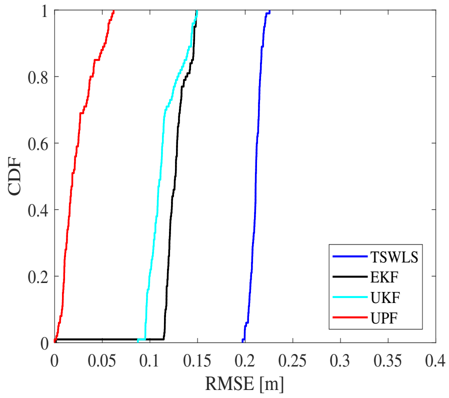

Figure 17. The CDF of RMSE for different algorithms in LOS scenario ($\sigma_{\theta_i} = 1^\circ$, $\sigma_{d_i} = 1$ m).

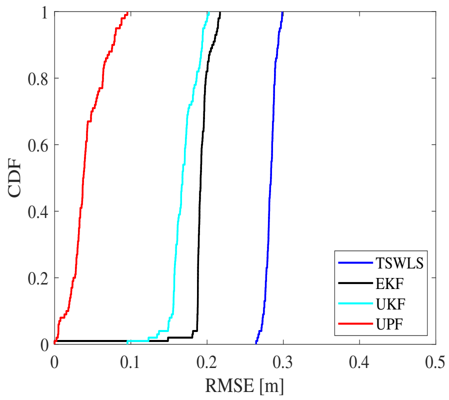

Figure 18. The CDF of RMSE for different algorithms in LOS scenario ($\sigma_{\theta_i} = 2^\circ$, $\sigma_{d_i} = 2$ m).

Table 3. The statistical parameters of positioning error in LOS scenarios.

Algorithm	$\sigma_{\theta_i} = 0.5^\circ$, $\sigma_{d_i} = 0.1$ m		$\sigma_{\theta_i} = 1^\circ$, $\sigma_{d_i} = 1$ m		$\sigma_{\theta_i} = 2^\circ$, $\sigma_{d_i} = 2$ m	
	Mean [m]	**Variance**	**Mean [m]**	**Variance**	**Mean [m]**	**Variance**
TSWLS	0.1341	0.0043	0.1987	0.0065	0.2675	0.0081
EKF	0.0882	0.0129	0.1137	0.0141	0.1699	0.0190
UKF	0.0797	0.0103	0.1018	0.0136	0.1533	0.0167
UPF	0.0101	0.0054	0.0241	0.0160	0.0418	0.0221

5.2.2. Curved Trajectory

When the trajectory of the target vehicle in the tunnel is a curve, we study the positioning performance of different algorithms. Figures 19 and 20 show the RMSE and the CDF of RMSE for $\sigma_{\theta_i} = 2^\circ$, $\sigma_{d_i} = 2$ m. When the trajectory of the target vehicle is curved, the proposed single-site positioning method can be utilized to estimate vehicle position effectively. The results illustrate that the localization performance of the positioning algorithm with a filter is better than the algorithm without a filter. All these simulation results theoretically verify the effectiveness of the proposed single-base station localization method.

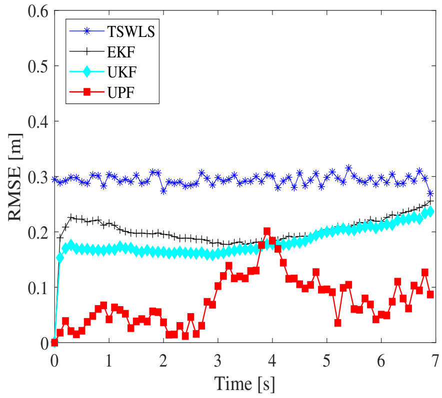

Figure 19. The RMSE of different algorithms in LOS scenario ($\sigma_{\theta_i} = 2^{\circ}$, $\sigma_{d_i} = 2$ m).

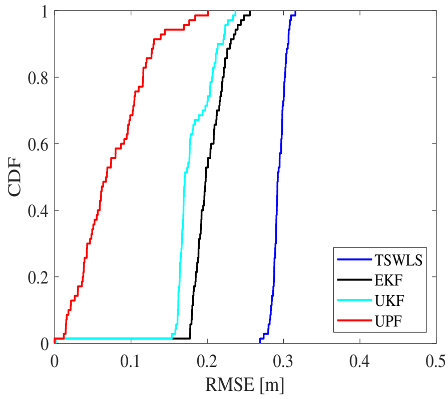

Figure 20. The CDF of RMSE for different algorithms in LOS scenario ($\sigma_{\theta_i} = 2^{\circ}$, $\sigma_{d_i} = 2$ m).

6. Conclusions

In this paper, we proposed a single-site positioning approach for the rectangular tunnel environment. In the proposed method, the NLOS paths are converted to LOS paths based on virtual station techniques; this simplifies the location complexity. In addition, only one base station is needed for vehicle localization; this reduces the cost of vehicle positioning. In NLOS scenarios, the joint TOA and DOA localization approach is exploited to calculate vehicle location. The TOA and DOA of the reflection paths from the tunnel walls are utilized to calculate the vehicle location. Moreover, the CRLB for the joint TOA and DOA localization method is derived. In the LOS scenarios, the LOS path and two reflection paths from the tunnel walls are used to obtain vehicle location. We calculate the vehicle location according to the DOA and TOA information of different paths. In addition, based on the localization algorithms with and without filters, the positioning performance is analyzed. Through the performance analysis and numerical simulations, it is shown that the proposed positioning approach provides a precise vehicle position in the tunnel environment. The positioning algorithms using filters could improve the positioning performance. The UPF positioning algorithm is better than EKF, UKF, and TSWLS algorithms in localization accuracy. In addition, the greater the measurement error, the greater the positioning error.

Author Contributions: Conceptualization, methodology and writing, S.J.; validation, W.W.; supervision, P.P. All authors have read and agreed to the published version of the manuscript.

Funding: This research was funded by Scientific Research Program Funded by Shaanxi Provincial Education Department (Program No. 22JK0248), the National Natural Science Foundation of China (Grant number 61871059), the Key Research and Development Program of Shaanxi (Program No. 2021KWZ-08), and the Innovation Capability Support Program of Shaanxi (Program No. 2022TD-41).

Institutional Review Board Statement: Not applicable.

Informed Consent Statement: Not applicable.

Data Availability Statement: Not applicable.

Conflicts of Interest: The authors declare no conflict of interest.

Appendix A. Derivation of CRLB for the Joint TOA and DOA Positioning

In this section, we focus on the derivation of the Fisher Information Matrix and CRLB.

$$
\begin{aligned}
\frac{\partial^2 L}{\partial^2 x} &= \frac{\partial L}{\partial x}\left(\frac{\partial}{\partial x}\left(-\sum_{i=1}^{N}\frac{1}{2}\left(\frac{\left(\hat{\theta}_i-\theta_i\right)^2}{{\sigma_{\theta_i}}^2}\right)\right)\right)+\frac{\partial L}{\partial x}\left(\frac{\partial}{\partial x}\left(-\sum_{i=1}^{N}\frac{1}{2}\left(\frac{\left(\hat{d}_i-d_i\right)^2}{{\sigma_{d_i}}^2}\right)\right)\right) \\
&= \frac{\partial L}{\partial x}\left(\frac{1}{2{\sigma_{\theta_i}}^2}\sum_{i=1}^{N}2\left(\hat{\theta}_i-\theta_i\right)\left(\frac{\partial \theta_i}{\partial x}\right)\right)+\frac{\partial L}{\partial x}\left(\frac{1}{2{\sigma_{d_i}}^2}\sum_{i=1}^{N}2\left(\hat{d}_i-d_i\right)\left(\frac{\partial d_i}{\partial x}\right)\right),
\end{aligned}
\tag{A1}
$$

where

$$
\frac{\partial \theta_i}{\partial x}=\frac{\partial}{\partial x}\left(\arctan\frac{y-y_{vi}}{x-x_{vi}}\right)=\frac{y-y_{vi}}{{d_i}^2},
\tag{A2}
$$

$$
\frac{\partial d_i}{\partial x}=\frac{\partial}{\partial x}\left(\sqrt{\left(x-x_{vi}\right)^2+\left(y-y_{vi}\right)^2}\right)=\frac{x-x_{vi}}{d_i}.
\tag{A3}
$$

Substituting Equation (A2) and Equation (A3) into Equation (A1), we have

$$
\begin{aligned}
\frac{\partial^2 L}{\partial^2 x} &= \frac{\partial L}{\partial x}\left(\frac{1}{2{\sigma_{\theta_i}}^2}\sum_{i=1}^{N}2\left(\hat{\theta}_i-\theta_i\right)\left(\frac{y-y_{vi}}{{d_i}^2}\right)\right)+\frac{\partial L}{\partial x}\left(\frac{1}{2{\sigma_{d_i}}^2}\sum_{i=1}^{N}2\left(\hat{d}_i-d_i\right)\left(\frac{x-x_{vi}}{d_i}\right)\right) \\
&= \sum_{i=1}^{N}\left(\frac{-\left(y-y_{vi}\right)^2}{{\sigma_{\theta_i}}^2{d_i}^4}-\frac{2\left(\hat{\theta}_i-\theta_i\right)\left(y-y_{vi}\right)\left(x-x_{vi}\right)}{{\sigma_{\theta_i}}^2{d_i}^4}\right) \\
&\quad +\sum_{i=1}^{N}\left(\frac{-\left(x-x_{vi}\right)^2}{{\sigma_{d_i}}^2{d_i}^2}+\frac{\left(\hat{d}_i-d_i\right)}{{\sigma_{d_i}}^2 d_i}\left(1-\frac{\left(x-x_{vi}\right)^2}{{d_i}^2}\right)\right),
\end{aligned}
\tag{A4}
$$

Since $\mathrm{E}\left(\hat{\theta}\right)=\theta$ and $\mathrm{E}\left(\hat{d}\right)=d$, therefore

$$
\mathrm{E}\left(\frac{\partial^2 L}{\partial^2 x}\right)=\sum_{i=1}^{N}\left(\frac{-\left(y-y_{vi}\right)^2}{{\sigma_{\theta_i}}^2{d_i}^4}\right)+\sum_{i=1}^{N}\left(\frac{-\left(x-x_{vi}\right)^2}{{\sigma_{d_i}}^2{d_i}^2}\right),
\tag{A5}
$$

$$
F_{xx}=\sum_{i=1}^{N}\left(\frac{\left(y-y_{vi}\right)^2}{{\sigma_{\theta_i}}^2{d_i}^4}\right)+\sum_{i=1}^{N}\left(\frac{\left(x-x_{vi}\right)^2}{{\sigma_{d_i}}^2{d_i}^2}\right)
\tag{A6}
$$

$$
\begin{aligned}
\frac{\partial^2 L}{\partial^2 y} &= \frac{\partial L}{\partial y}\left(\frac{\partial}{\partial y}\left(-\sum_{i=1}^{N}\frac{1}{2}\left(\frac{\left(\hat{\theta}_i-\theta_i\right)^2}{{\sigma_{\theta_i}}^2}\right)\right)\right)+\frac{\partial L}{\partial y}\left(\frac{\partial}{\partial y}\left(-\sum_{i=1}^{N}\frac{1}{2}\left(\frac{\left(\hat{d}_i-d_i\right)^2}{{\sigma_{d_i}}^2}\right)\right)\right) \\
&= \frac{\partial L}{\partial y}\left(\frac{1}{2{\sigma_{\theta_i}}^2}\sum_{i=1}^{N}2\left(\hat{\theta}_i-\theta_i\right)\left(\frac{\partial \theta_i}{\partial y}\right)\right)+\frac{\partial L}{\partial y}\left(\frac{1}{2{\sigma_{d_i}}^2}\sum_{i=1}^{N}2\left(\hat{d}_i-d_i\right)\left(\frac{\partial d_i}{\partial y}\right)\right),
\end{aligned}
\tag{A7}
$$

with

$$
\frac{\partial \theta_i}{\partial y}=\frac{\partial}{\partial y}\left(\arctan\frac{y-y_{vi}}{x-x_{vi}}\right)=\frac{x-x_{vi}}{{d_i}^2},
\tag{A8}
$$

$$
\frac{\partial d_i}{\partial y}=\frac{\partial}{\partial y}\left(\sqrt{\left(x-x_{vi}\right)^2+\left(y-y_{vi}\right)^2}\right)=\frac{y-y_{vi}}{d_i}.
\tag{A9}
$$

Substituting Equation (A8) and Equation (A9) into Equation (A7), we get

$$\begin{aligned}
\frac{\partial^2 L}{\partial^2 y} &= \frac{\partial L}{\partial y}\left(\frac{1}{2\sigma_{\theta_i}{}^2}\sum_{i=1}^{N}2\left(\hat{\theta}_i-\theta_i\right)\left(\frac{x-x_{vi}}{d_i{}^2}\right)\right)+\frac{\partial L}{\partial y}\left(\frac{1}{2\sigma_{d_i}{}^2}\sum_{i=1}^{N}2\left(\hat{d}_i-d_i\right)\left(\frac{y-y_{vi}}{d_i}\right)\right)\\
&= \sum_{i=1}^{N}\left(-\frac{(x-x_{vi})^2}{\sigma_{\theta_i}{}^2 d_i{}^4}-\frac{2\left(\hat{\theta}_i-\theta_i\right)(x-x_{vi})(y-y_{vi})}{\sigma_{\theta_i}{}^2 d_i{}^4}\right)\\
&\quad+\sum_{i=1}^{N}\left(-\frac{(y-y_{vi})^2}{\sigma_{d_i}{}^2 d_i{}^2}+\frac{\left(\hat{d}_i-d_i\right)\left(d_i{}^2-(y-y_{vi})^2\right)}{\sigma_{d_i}{}^2 d_i{}^3}\right).
\end{aligned} \tag{A10}$$

Since $\mathrm{E}\left(\hat{\theta}\right)=\theta$ and $\mathrm{E}\left(\hat{d}\right)=d$, therefore

$$\mathrm{E}\left(\frac{\partial^2 L}{\partial^2 y}\right)=\sum_{i=1}^{N}\left(-\frac{(x-x_{vi})^2}{\sigma_{\theta_i}{}^2 d_i{}^4}\right)+\sum_{i=1}^{N}\left(-\frac{(y-y_{vi})^2}{\sigma_{d_i}{}^2 d_i{}^2}\right). \tag{A11}$$

$$F_{yy}=\sum_{i=1}^{N}\left(\frac{(x-x_{vi})^2}{\sigma_{\theta_i}{}^2 d_i{}^4}\right)+\sum_{i=1}^{N}\left(\frac{(y-y_{vi})^2}{\sigma_{d_i}{}^2 d_i{}^2}\right). \tag{A12}$$

$$\begin{aligned}
\frac{\partial L}{\partial y}\left(\frac{\partial L}{\partial x}\right) &= \frac{\partial L}{\partial y}\left(\frac{\partial}{\partial x}\left(-\sum_{i=1}^{N}\frac{1}{2}\left(\frac{\left(\hat{\theta}_i-\theta_i\right)^2}{\sigma_{\theta_i}{}^2}\right)\right)\right)+\frac{\partial L}{\partial y}\left(\frac{\partial}{\partial x}\left(-\sum_{i=1}^{N}\frac{1}{2}\left(\frac{\left(\hat{d}_i-d_i\right)^2}{\sigma_{d_i}{}^2}\right)\right)\right)\\
&= \frac{\partial L}{\partial y}\left(\frac{1}{2\sigma_{\theta_i}{}^2}\sum_{i=1}^{N}2\left(\hat{\theta}_i-\theta_i\right)\left(\frac{\partial\theta_i}{\partial x}\right)\right)+\frac{\partial L}{\partial y}\left(\frac{1}{2\sigma_{d_i}{}^2}\sum_{i=1}^{N}2\left(\hat{d}_i-d_i\right)\left(\frac{\partial d_i}{\partial x}\right)\right)\\
&= \frac{\partial L}{\partial y}\left(\frac{1}{\sigma_{\theta_i}{}^2}\sum_{i=1}^{N}\left(\hat{\theta}_i-\theta_i\right)\left(\frac{y-y_{vi}}{d_i{}^2}\right)\right)+\frac{\partial L}{\partial y}\left(\frac{1}{\sigma_{d_i}{}^2}\sum_{i=1}^{N}\left(\hat{d}_i-d_i\right)\left(\frac{x-x_{vi}}{d_i}\right)\right)\\
&= \sum_{i=1}^{N}\left(\frac{-(x-x_{vi})(y-y_{vi})}{\sigma_{\theta_i}{}^2 d_i{}^4}+\frac{\left(\hat{\theta}_i-\theta_i\right)\left(d_i{}^2-2(y-y_{vi})^2\right)}{\sigma_{\theta_i}{}^2 d_i{}^4}\right)\\
&\quad+\sum_{i=1}^{N}\left(\frac{-(x-x_{vi})(y-y_{vi})}{\sigma_{d_i}{}^2 d_i{}^2}-\frac{\left(\hat{d}_i-d_i\right)(x-x_{vi})(y-y_{vi})}{\sigma_{d_i}{}^2 d_i{}^3}\right).
\end{aligned} \tag{A13}$$

Since $\mathrm{E}\left(\hat{\theta}\right)=\theta$ and $\mathrm{E}\left(\hat{d}\right)=d$, therefore

$$\mathrm{E}\left(\frac{\partial L}{\partial y}\left(\frac{\partial L}{\partial x}\right)\right)=-\sum_{i=1}^{N}\left(\frac{(x-x_{vi})(y-y_{vi})}{\sigma_{\theta_i}{}^2 d_i{}^4}\right)-\sum_{i=1}^{N}\left(\frac{(x-x_{vi})(y-y_{vi})}{\sigma_{d_i}{}^2 d_i{}^2}\right). \tag{A14}$$

Due to $\frac{\partial L}{\partial y}\left(\frac{\partial L}{\partial x}\right)=\frac{\partial L}{\partial x}\left(\frac{\partial L}{\partial y}\right)$, therefore

$$\mathrm{E}\left(\frac{\partial L}{\partial x}\left(\frac{\partial L}{\partial y}\right)\right)=-\sum_{i=1}^{N}\left(\frac{(x-x_{vi})(y-y_{vi})}{\sigma_{\theta_i}{}^2 d_i{}^4}\right)-\sum_{i=1}^{N}\left(\frac{(x-x_{vi})(y-y_{vi})}{\sigma_{d_i}{}^2 d_i{}^2}\right). \tag{A15}$$

$$F_{xy}=F_{yx}=\sum_{i=1}^{N}\left(\frac{(x-x_{vi})(y-y_{vi})}{\sigma_{\theta_i}{}^2 d_i{}^4}\right)+\sum_{i=1}^{N}\left(\frac{(x-x_{vi})(y-y_{vi})}{\sigma_{d_i}{}^2 d_i{}^2}\right). \tag{A16}$$

$$CRLB=tr\left(\mathbf{F}^{-1}\right)=\frac{F_{xx}+F_{yy}}{F_{xx}F_{yy}-F_{xy}F_{yx}}, \tag{A17}$$

Putting Equation (A6), Equation (A12), and Equation (A16) into (A17), we can obtain the CRLB.

References

1. Golestan, K.; Sattar, F.; Karray, F.; Kamel, M.; Seifzadeh, S. Localization in vehicular ad hoc networks using data fusion and V2V communication. *Comput. Commun.* **2015**, *71*, 61–72. [CrossRef]
2. Jiang, S.; Wang, W.; Rashdan, I. V2V channel modeling at 5.2 GHz for highway environment. *China Commun.* **2022**, *19*, 112–128. [CrossRef]
3. Lee, M.; Atkison, T. VANET applications: Past, present, and future. *Veh. Commun.* **2021**, *28*, 100310–100355. [CrossRef]
4. Mokhtar, B.; Azab, M. Survey on security issues in vehicular ad hoc networks. *Alex. Eng. J.* **2015**, *54*, 1115–1126. [CrossRef]
5. Toor, Y.; Muhlethaler, P.; Laouiti, A.; De La Fortelle, A. Vehicle ad hoc networks: Applications and related technical issues. *IEEE Commun. Surv. Tutor.* **2008**, *10*, 74–88. [CrossRef]
6. Balico, L.N.; Loureiro, A.A.; Nakamura, E.F.; Barreto, R.S.; Pazzi, R.W.; Oliveira, H.A. Localization prediction in vehicular ad hoc networks. *IEEE Commun. Surv. Tutor.* **2018**, *20*, 2784–2803. [CrossRef]
7. Günay, F.B.; Öztürk, E.; Çavdar, T.; Hanay, Y.S. Vehicular ad hoc network (VANET) localization techniques: A survey. *Arch. Comput. Methods Eng.* **2021**, *28*, 3001–3033. [CrossRef]
8. Drawil, N.M.; Basir, O. Intervehicle-communication-assisted localization. *IEEE Trans. Intell. Transp. Syst.* **2010**, *11*, 678–691. [CrossRef]
9. Ghaleb, F.A.; Zainal, A.; Rassam, M.A.; Abraham, A. Improved vehicle positioning algorithm using enhanced innovation-based adaptive Kalman filter. *Pervasive Mob. Comput.* **2017**, *40*, 139–155. [CrossRef]
10. Rohani, M.; Gingras, D.; Vigneron, V.; Gruyer, D. A new decentralized Bayesian approach for cooperative vehicle localization based on fusion of GPS and VANET based inter-vehicle distance measurement. *IEEE Intell. Transp. Syst. Mag.* **2015**, *7*, 85–95. [CrossRef]
11. Abumansoor, O.; Boukerche, A. A secure cooperative approach for nonline-of-sight location verification in VANET. *IEEE Trans. Veh. Technol.* **2011**, *61*, 275–285. [CrossRef]
12. Boukerche, A.; Oliveira, H.A.; Nakamura, E.F.; Loureiro, A.A. Vehicular ad hoc networks: A new challenge for localization-based systems. *Comput. Commun.* **2008**, *31*, 2838–2849. [CrossRef]
13. Qureshi, K.N.; Abdullah, A.H. Localization-based system challenges in vehicular ad hoc networks: survey. *Smart Comput. Rev.* **2014**, *4*, 515–528.
14. Fang, F.; Ding, Z. High precision positioning and accident detection system for vehicles in traffic tunnel. In Proceedings of the 2019 IEEE 2nd International Conference on Electronic Information and Communication Technology (ICEICT), Harbin, China, 20–22 January 2019; pp. 419–425.
15. Ling, J.; Wang, L.; Ji, H.; Xie, H.; Ding, J.; Dai, Q. UWB-based real-time continuous positioning system in NLOS tunnel environment. In Proceedings of the 2018 International Conference on Cyber-Enabled Distributed Computing and Knowledge Discovery (CyberC), Zhengzhou, China, 18–20 October 2018; pp. 142–1424.
16. Cypriani, M.; Delisle, G.; Hakem, N. Wi-Fi-based positioning in underground mine tunnels. In Proceedings of the International Conference on Indoor Positioning and Indoor Navigation, Montbeliard, France, 28–31 October 2013; pp. 1–7.
17. Kim, K.; Im, J.; Jee, G. Tunnel facility based vehicle localization in highway tunnel using 3D LIDAR. *IEEE Trans. Intell. Transp. Syst.* **2022**, *23*, 17575–17583. [CrossRef]
18. Wang, Y.; Yin, X.; Cai, G.; Wang, G.; Guo, S.; Liang, K. Tunnel vehicle RSSI positioning algorithm based on LMLF model. In Proceedings of the 2019 4th International Conference on Cloud Computing and Internet of Things (CCIOT), Changchun, China, 6–7 December 2019; pp. 29–32.
19. Agarwal, Y.; Jain, K.; Kumar, S.; Bhardwaj, G.N. TLST: Time of arrival based localization and smart tunnel concept in VANETs. In Proceedings of the 2016 3rd International Conference on Signal Processing and Integrated Networks (spin), Noida, India, 11–12 February 2016; pp. 763–768.
20. Savic, V.; Wymeersch, H.; Larsson, E.G. Simultaneous sensor localization and target tracking in mine tunnels. In Proceedings of the 16th International Conference on Information Fusion, Istanbul, Turkey, 9–12 July 2013; pp. 1427–1433.
21. Zhang, L.C.; Yu, T.T.; Wang, M. Research on Vehicles Position Evaluation Algorithm of Highway Tunnel. In *Proceedings of the Advanced Materials Research*; Trans Tech Publ.: Zurich, Switzerland, 2013; Volume 718, pp. 1618–1623.
22. Yan, T.; Zhang, W.; Wang, G.; Zhang, Y. GOT: Grid-based on-road localization through inter-vehicle collaboration. In Proceedings of the 2011 IEEE Eighth International Conference on Mobile Ad-Hoc and Sensor Systems, Valencia, Spain, 17–22 October 2011; pp. 13–18.
23. Shin, B.; Lee, J.H.; Yu, C.; Kyung, H.; Lee, T. Magnetic Field-Based Vehicle Positioning System in Long Tunnel Environment. *Appl. Sci.* **2021**, *11*, 11641–11656. [CrossRef]
24. Song, X.; Li, X.; Tang, W.; Zhang, W.; Li, B. A hybrid positioning strategy for vehicles in a tunnel based on RFID and in-vehicle sensors. *Sensors* **2014**, *14*, 23095–23118. [CrossRef]
25. Hoang, G.M.; Denis, B.; Härri, J.; Slock, D.T. Robust data fusion for cooperative vehicular localization in tunnels. In Proceedings of the 2017 IEEE Intelligent Vehicles Symposium (IV), Los Angeles, CA, USA, 11–14 June 2017; pp. 1372–1377.
26. Halili, R.; BniLam, N.; Yusuf, M.; Tanghe, E.; Joseph, W.; Weyn, M.; Berkvens, R. Vehicle Localization Using Doppler Shift and Time of Arrival Measurements in a Tunnel Environment. *Sensors* **2022**, *22*, 847–866. [CrossRef]
27. Mageid, S.A. Connectivity based positioning system for underground vehicular ad hoc networks. *Int. J. Comput. Netw. Appl.* **2017**, *4*, 1–14. [CrossRef]
28. Ulmschneider, M.; Gentner, C. Multipath assisted positioning for pedestrians using LTE signals. In Proceedings of the 2016 IEEE/ION Position, Location and Navigation Symposium (PLANS), Savannah, GA, USA, 11–14 April 2016; pp. 386–392.

29. Gentner, C.; Jost, T.; Wang, W.; Zhang, S.; Dammann, A.; Fiebig, U.C. Multipath assisted positioning with simultaneous localization and mapping. *IEEE Trans. Wirel. Commun.* **2016**, *15*, 6104–6117. [CrossRef]
30. Karásek, R.; Gentner, C. Stochastic data association for multipath assisted positioning using a single transmitter. *IEEE Access* **2020**, *8*, 46735–46752. [CrossRef]
31. Ulmschneider, M.; Zhang, S.; Gentner, C.; Dammann, A. Multipath assisted positioning with transmitter visibility information. *IEEE Access* **2020**, *8*, 155210–155223. [CrossRef]
32. Ulmschneider, M.; Gentner, C.; Jost, T.; Dammann, A. Multiple hypothesis data association for multipath-assisted positioning. In Proceedings of the 2017 14th Workshop on Positioning, Navigation and Communications (WPNC), Bremen, Germany, 25–26 October 2017; pp. 1–6.
33. Song, X.; Li, X.; Tang, W.; Zhang, W. RFID/in-vehicle sensors-integrated vehicle positioning strategy utilising LSSVM and federated UKF in a tunnel. *J. Navig.* **2016**, *69*, 845–868. [CrossRef]
34. Qin, Y.; Zhou, C.; Yang, S.H.; Wang, F. A distributed newton iteration based localization scheme in underground tunnels. In Proceedings of the 2012 UKACC International Conference on Control, Cardiff, UK, 3–5 September 2012; pp. 851–856.
35. Li, C.R.; Xie, J.L.; Yang, L.L. Angle offset-assisted positioning of railway vehicles in tunnel environments. In Proceedings of the 2015 IEEE 81st Vehicular Technology Conference (VTC Spring), Glasgow, UK, 11–14 May 2015; pp. 1–5.
36. Wang, B.; Sun, D.; Zu, H.; Wu, C.; Zhang, D.; Chen, X. *Fusion Positioning System Based on IMU and Roadside LiDAR in Tunnel for C-V2X Use*; Technical report; SAE Technical Paper; 2020.
37. Kong, X.; Li, X.; Song, X.; Tian, Y.; Kong, D. An accurate and reliable positioning methodology for land vehicles in tunnels based on UWB/INS integration. *Meas. Sci. Technol.* **2022**, *33*, 1–10. [CrossRef]
38. Islam, A.; Hossain, M.A.; Le, N.T.; Hong, C.H.; Nguyen, T.; Jang, Y.M. Precise Localization in Tunnel Environment using Visible Light Communication. In Proceedings of the 26th Joint Conference on Communications and Information, Lisbon, Portugal, 19–25 August 2016; pp. 26–28.
39. Kim, B.W.; Jung, S.Y. Vehicle positioning scheme using V2V and V2I visible light communications. In Proceedings of the 2016 IEEE 83rd Vehicular Technology Conference (VTC Spring), Nanjing, China, 15–18 May 2016; pp. 1–5.
40. de Ponte Müller, F. Survey on ranging sensors and cooperative techniques for relative positioning of vehicles. *Sensors* **2017**, *17*, 271–297. [CrossRef]
41. Jaffe, A.; Wax, M. Single-site localization via maximum discrimination multipath fingerprinting. *IEEE Trans. Signal Process.* **2014**, *62*, 1718–1728. [CrossRef]
42. Jost, T.; Wang, W.; Fiebig, U.C.; Perez-Fontan, F. Detection and tracking of mobile propagation channel paths. *IEEE Trans. Antennas Propag.* **2012**, *60*, 4875–4883. [CrossRef]
43. Jiang, S.; Wang, W.; Jost, T.; Peng, P.; Sun, Y. An ARMA-filter based SAGE algorithm for ranging in diffuse scattering environment. *IEEE Trans. Veh. Technol.* **2022**, *71*, 3361–3366. [CrossRef]
44. Liang, J.; He, J.; Yu, W.; Truong, T.K. Single-Site 3-D Positioning in Multipath Environments Using DOA-Delay Measurements. *IEEE Commun. Lett.* **2021**, *25*, 2559–2563. [CrossRef]
45. Liu, D.; Liu, K.; Ma, Y.; Yu, J. Joint TOA and DOA Localization in Indoor Environment Using Virtual Stations. *IEEE Commun. Lett.* **2014**, *18*, 1423–1426. [CrossRef]
46. Zhang, R.; Xia, W.; Yan, F.; Shen, L. A single-site positioning method based on TOA and DOA estimation using virtual stations in NLOS environment. *China Commun.* **2019**, *16*, 146–159.
47. Zhang, R.; Chen, G.; Zeng, Q.; Shen, L. Single-Site Positioning Method Based on High-Resolution Estimation in VANET Localization. *IEEE Access* **2018**, *6*, 54674–54682. [CrossRef]
48. J. Youn.; J. Jo.; D. K. Kim. Study on Crammer-Rao Lower Bound of Angle-of-Arrival Position Estimation for Cooperative Vehicle-to-Vehicle (V2V) Communication. In Proceedings of the 2018 International Conference on Information and Communication Technology Convergence (ICTC), Jeju Island, Korea, 17–19 October 2018; pp. 1–4.
49. Kang, Y.; Wang, Q.; Wang, J.; Chen, R. A high-accuracy TOA-based localization method without time synchronization in a three-dimensional space. *IEEE Trans. Ind. Inform.* **2018**, *15*, 173–182. [CrossRef]
50. Rui, Y.; Chen, Y. Better proposal distributions: Object tracking using unscented particle filter. In Proceedings of the Proceedings of the 2001 IEEE Computer Society Conference on Computer Vision and Pattern Recognition, CVPR 2001, Kauai, HI, USA, 8–14 December 2001; Volume 2, pp. 786–793.
51. Van Der Merwe, R.; Doucet, A.; De Freitas, N.; Wan, E. *The Unscented Particle Filter*; Technical Report CUED/F-INFENG/TR 380; Cambridge University Engineering Department: Cambridge, UK, 2000 .
52. Wan, E.A.; Van Der Merwe, R. The unscented Kalman filter for nonlinear estimation. In Proceedings of the IEEE 2000 Adaptive Systems for Signal Processing, Communications, and Control Symposium, Lake Louise, AB, Canada, 4 October 2000; pp. 153–158.
53. Wu, H.; Liang, L.; Mei, X.; Zhang, Y. A convex optimization approach for NLOS error mitigation in TOA-based localization. *IEEE Signal Process. Lett.* **2022**, *29*, 677–681. [CrossRef]
54. Seow, C.K.; Tan, S.Y. Non-line-of-sight localization in multipath environments. *IEEE Trans. Mob. Comput.* **2008**, *7*, 647–660. [CrossRef]